Molecular Vision 2012; 18:1031-1039 <http://www.molvis.org/molvis/v18/a109>
Received 27 November 2011 | Accepted 20 April 2012 | Published 24 April 2012

A new mutation in the *RP1L1* gene in a patient with occult macular dystrophy associated with a depolarizing pattern of focal macular electroretinograms

Takenori Kabuto,[1] Hisatomo Takahashi,[1] Yoko Goto-Fukuura,[1] Tsutomu Igarashi,[2] Masakazu Akahori,[3] Shuhei Kameya,[1] Takeshi Iwata,[3] Atsushi Mizota,[4] Kunihiko Yamaki,[1] Yozo Miyake,[5,6] Hiroshi Takahashi[2]

[1]Department of Ophthalmology, Nippon Medical School Chiba Hokusoh Hospital, Chiba, Japan; [2]Department of Ophthalmology, Nippon Medical School, Tokyo, Japan; [3]Division of Molecular & Cellular Biology, National Institute of Sensory Organs, National Hospital Organization Tokyo Medical Center, Tokyo, Japan; [4]Department of Ophthalmology, Teikyo University School of Medicine, Tokyo, Japan; [5]Department of Ophthalmology, National Institute of Sensory Organs, National Hospital Organization Tokyo Medical Center, Tokyo, Japan; [6]Aichi Medical University, 21 Yazakokarimata, Nagakute-cho, Aichi, Japan

Purpose: To determine whether a mutation in the RP1-like protein 1 (*RP1L1*) gene is present in a Japanese patient with sporadic occult macular dystrophy (OMD) and to examine the characteristics of focal macular electroretinograms (ERGs) of the patient with genetically identified OMD.

Methods: An individual with OMD underwent detailed ophthalmic clinical evaluations including focal macular ERGs. Mutation screening of all coding regions and flanking intron sequences of the *RP1L1* gene were performed with DNA sequencing analysis in this case with OMD.

Results: A new *RP1L1* mutation (c.3596 C>G in exon 4) was identified. The variant c.3596 C>G in exon 4 resulted in the substitution of cysteine for serine at amino acid position 1199. The serine at position 1199 is well conserved among the RP1L1 family in other species. Four out of five computational assessment tools predicted that this mutation is damaging to the protein function. This mutation was not present in 294 control alleles. The waveform of focal macular ERGs recorded from the patient with OMD had a depolarizing pattern, simulating the ERG waveforms observed after the hyperpolarizing bipolar cell activity is blocked.

Conclusions: We have demonstrated in a Japanese patient the possibility that sporadic OMD may also be caused by an *RP1L1* mutation. The waveform of focal macular ERGs elicited from the OMD patient with the *RP1L1* mutation showed a depolarizing pattern. This characteristic is the same as reported for the focal macular ERGs of OMD.

Occult macular dystrophy (OMD; OMIM 613587) is an inherited macular dystrophy characterized by a progressive decrease in visual acuity with an essentially normal fundus and normal fluorescein angiograms [1,2]. The full-field electroretinograms (ERGs) are normal; however, the focal macular ERGs and multifocal ERGs (mfERGs) recorded from the macular area are abnormal [1-3]. Despite normal ophthalmoscopic findings, spectral domain-optical coherence tomography (SD-OCT) has shown morphological changes in the retina in the macular area [4-8]. Several studies have reported various degrees of disruption of the inner segment/outer segment (IS/OS) junction and the cone outer segment tip (COST) line [4-8].

The hereditary form of OMD is an autosomal dominant trait; however, sporadic patients have also been reported [3, 9]. The gene responsible for the disease was recently identified as the RP1-like protein 1 (*RP1L1*) in four families with autosomal dominant OMD [10]. The *RP1L1* gene has been identified through sequence analyses of human and mouse genomes [11,12]. The human *RP1L1* gene is encoded in four exons that span 50 kb on chromosome 8p. The length of the mRNA of *RP1L1* is more than 7 kb, but the exact length varies among individuals because of the presence of several length polymorphisms. *RP1L1* encodes a protein with a minimal length of 2,400 amino acids and a predicted weight of 252 kDa.

The expression of RP1L1 is limited to the retina, and appears to be specific to photoreceptors [12]. The *RP1L1* gene was also found to be conserved in distant vertebrates [11]. Knockout mice lacking the RP1L1 protein have reduced ERG amplitudes and progressive photoreceptor degeneration [13]. The study of *RP1L1*$^{-/-}$ mice also showed that the RP1L1 protein is located in the axoneme of the outer segments and connecting cilia exclusively in rod photoreceptors. The RP1L1 protein appears not to be expressed in cone photoreceptors in mice, although more than 97% of the photoreceptors in mice are rods [13]. However, immunohistochemical analysis of the RP1L1 of Cynomolgus monkeys with the human RP1L1 antibody showed that RP1L1

Correspondence to: Shuhei Kameya, Department of Ophthalmology, Nippon Medical School Chiba Hokusoh Hospital, 1715 Kamagari, Inzai, Chiba 270-1694, Japan; Phone: +81 476 99 1111; FAX: +81 476 99 1923; email: shuheik@nms.ac.jp

was expressed in rod and cone photoreceptors [10]. Because the amino acid sequence of human RP1L1 is only 39% identical to that of the mouse, researchers have suggested that the primate RP1L1 might have different functional roles in the cone photoreceptors of the retina than that of other species [10].

We have identified a new mutation in the *RP1L1* gene in a patient with clinical characteristics of OMD: abnormal focal macular ERGs and blurring of the IS/OS junction and the disappearance of the COST line in SD-OCT images. The fundus examination, fluorescein angiograms, and full-field ERGs were normal in this case. The mutation is an amino acid substitution of cysteine for serine in exon 4 of the *RP1L1* gene that has not been reported in the Single Nucleotide Polymorphism (SNP) database and was also not detected in any of the 294 normal control alleles. The serine at position 1199 is well conserved among the RP1L1 family in other species. Four out of five computational assessment tools (PolyPhen-2, SIFT, PMut, Align GVGD, and MutationTaster) predicted that this mutation is damaging to the protein function. A segregation of the mutation and the disease was found in one affected member and one unaffected member of the same family.

METHODS

The protocol conformed to the tenets of the Declaration of Helsinki and was approved by the Institutional Review Board of the Nippon Medical School and the ethics review committees of the National Hospital Organization Tokyo Medical Center. Written informed consent was obtained from all patients after the nature and possible consequences of the study were explained.

Clinical studies: The ophthalmological examinations included best-corrected visual acuity (BCVA) measurements, refraction, slit-lamp biomicroscopy, ophthalmoscopy, fundus photography, perimetry, SD-OCT, fluorescein angiography (FA), full-field ERGs, focal ERGs, and mfERGs. The visual fields were determined with the Goldman perimetry and the Humphrey Visual Field Analyzer (model 745i; Carl Zeiss Meditec, Inc., Dublin, CA). The Swedish interactive threshold algorithm standard strategy was used with program 30–2 of the Humphrey Visual Field Analyzer. The OCT images were recorded using a SD-OCT (Carl Zeiss Meditec) on this patient and normal controls. Full-field scotopic and photopic ERGs were recorded using an extended testing protocol incorporating the International Society for Clinical Electrophysiology of Vision standards [14]. The full-field ERGs were used to assess retinal function under scotopic and photopic states.

Focal macular electroretinograms: Focal macular ERGs were recorded with a commercial Focal Macular ERG system (ER80; Kowa Company, Tokyo, Japan, and PuREC; Mayo Company, Nagoya, Japan) using a bipolar contact lens electrode (MY type Electrode; Mayo Company). The stimulus and background lights were integrated into an infrared fundus camera [15-17]. The size of the stimulus spot was 15° in diameter and was placed on the macula by observing the infrared image of the retina on a monitor. The white stimulus and background illumination were generated by light-emitting diodes that had maximal spectral emissions at 440 to 460 nm and 550 to 580 nm, respectively. The luminances of the stimuli and background were 115.7 cd/m^2 and 8.0 cd/m^2. The duration of the stimulation was 100 ms. The responses were amplified and filtered with digital band pass filters from 5 to 200 Hz. Three hundred responses were summed with a stimulus frequency of 5 Hz. The a-wave, b-wave, d-wave, and oscillatory potentials (OPs) were evaluated.

Multifocal electroretinograms: The mfERGs were recorded using a commercial mfERG system (LE-4000, Tomey, Nagoya, Japan; LE4100; Mayo Company, Inazawa, Japan). This system uses basically the same technology as the Visual Evoked Response Imaging System [18]. The visual stimuli consisted of 37 hexagonal elements with an overall subtense of approximately 50°. The luminance of each hexagon was independently modulated between black (2.47 cd/m^2) and white (200.4 cd/m^2) according to a binary m-sequence at 75 Hz. The surround luminance was set at 75.4 cd/m^2.

Mutation analysis: Blood samples were collected from the patient, and genomic DNA was isolated from peripheral white blood cells using a blood DNA isolation kit (NucleoSpin Blood XL; Macherey Nagel, Düren, Germany). The DNA was used as the template to amplify the *RP1L1* gene. Coding regions and flanking introns of the *RP1L1* gene were amplified with polymerase chain reaction (PCR) using primers produced by Greiner Bio-One (Tokyo, Japan). Primer sequences are listed in Table 1. The PCR products were purified (ExoSAP-IT; USB Corp., Cleveland, OH) and were used as the template for sequencing. Both strands were sequenced on an automated sequencer (Bio Matrix Research; Chiba, Japan). The identified mutations and coding polymorphisms were assayed in 294 control chromosomes from 147 healthy Japanese individuals with direct sequencing except the length polymorphism region. To sequence the length polymorphism region of the *RP1L1* gene, the amplified PCR products were subcloned into the StrataClone PCR cloning vector (Stratagene; La Jolla, CA). At least five cloned products from this case and 20 control individuals were sequenced on an automated sequencer.

Computational assessment of missense mutation: The effect of a missense mutation on the encoded protein was predicted with the PolyPhen-2, SIFT, PMut, Align GVGD, and MutationTaster online tools [19-24]. PolyPhen-2 is a software tool that predicts the possible impact of amino acid substitutions on the structure and function of human proteins using straightforward physical and evolutionary comparative

Table 1. Sequences of oligonucleotide primers used in this study and PCR product size.

Fragment name	Forward primer (5′-3′)	Reverse primer (5′-3′)	Product size (bp)
RP1L1–2A	GAGACAGGAAATGCCAATCC	CCGCAACTGCTGAGCAGTGG	471
RP1L1–2B	CCTCTGCTCTGATAAGAAGC	TCCATGTGAGTATTTTGACC	373
RP1L1–3	CCTCCAGCTAGTGATAGAGG	GATTGACAGTACTGAGAAGG	498
RP1L1–4A	TTCCTTTATCCTGATGCTGC	CCAAAGACTTCCCTGCATCC	509
RP1L1–4B	TGTGGGAGGGCTACCCTTGG	GCTGACGAGTCCGAAGAAGC	508
RP1L1–4C	CTATGCATAGATGGAGCAGG	GTTACAGAGGAGTCCAGTGG	536
RP1L1–4D	CAATGTCCTCACCCAGCAGC	TCCAACCTGCAGAACCAAGG	494
RP1L1–4E	GACTCCTGCTCAAAATCTGG	GGACACCCTCTCCTGATTGG	784
RP1L1–4F	GGACAGCAGTCCCTGGAAGG	ACTGCACCGCCTCTTCTTGC	937
RP1L1–4G	AAACACAGTGCAAGAAGAGG	AGGCTCAAGCTGGGAGCCACTCTGC	variable
RP1L1–4H	GGGAAAGGCTCCCAGGAAGATGACC	TTCTGCACCTTCTGACTCTGGCTGG	1470
RP1L1–4I	CACAGAGGAACCCACAGAGC	GAGAAGGCCGAGAGGTTTCG	522
RP1L1–4J	CAAGAGAGAGCTCCAGAAGC	TCTGTTGAGTCTCTGGCTCC	547
RP1L1–4K	GACAAAGATCCCAAACTCGG	AGAGTCAGAAGATGTAGAGG	836
RP1L1–4L	TGAAGGGGAGATGCAAGAGG	GAGTGGGCCTGTCCTCAGGGACTGG	821
RP1L1–4M	AGGCTTCTGAAAGCAGCAGC	ACTATGGACATCTCCAGTGG	517

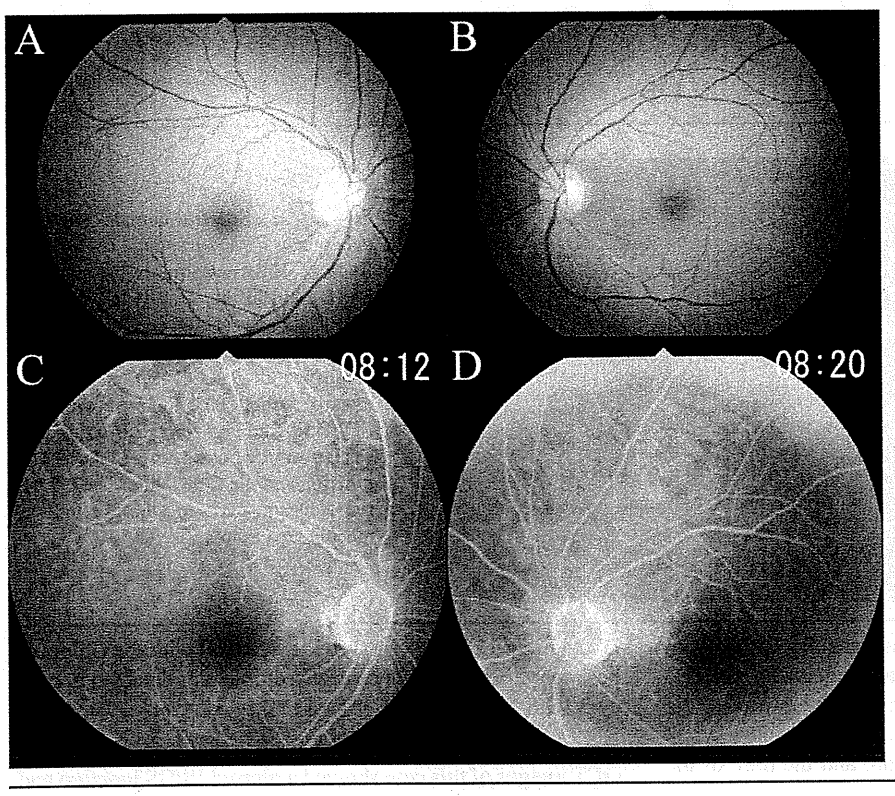

Figure 1. Fundus photographs (**A**, **B**) and fluorescein angiograms (**C**, **D**) of this case showing no abnormal findings.

considerations. SIFT generates multiple alignments of the sequence over different species to look at the conserved sequences of a gene; it assesses the conserved amino acid positions and analyzes the effect of missense changes on the conserved structure of proteins over the course of evolution. The SIFT tool assigns a score to the mutations, and a score of <0.05 is considered potentially damaging. PMut is software aimed at annotating and predicting pathological mutations. Align GVGD combines the biophysical characteristics of amino acids and protein multiple sequence alignments to predict where missense substitutions in genes of interest fall in a spectrum from enriched deleterious to enriched neutral. MutationTaster evaluates the disease-causing potential of sequence alterations.

Statistical analysis: We calculated the 95% confidence intervals (CI) of the results of the focal macular ERGs of normal controls. There were 25 men and 21 women whose age ranged from 23 to 60 years (mean, 38.04±8.33 years) in

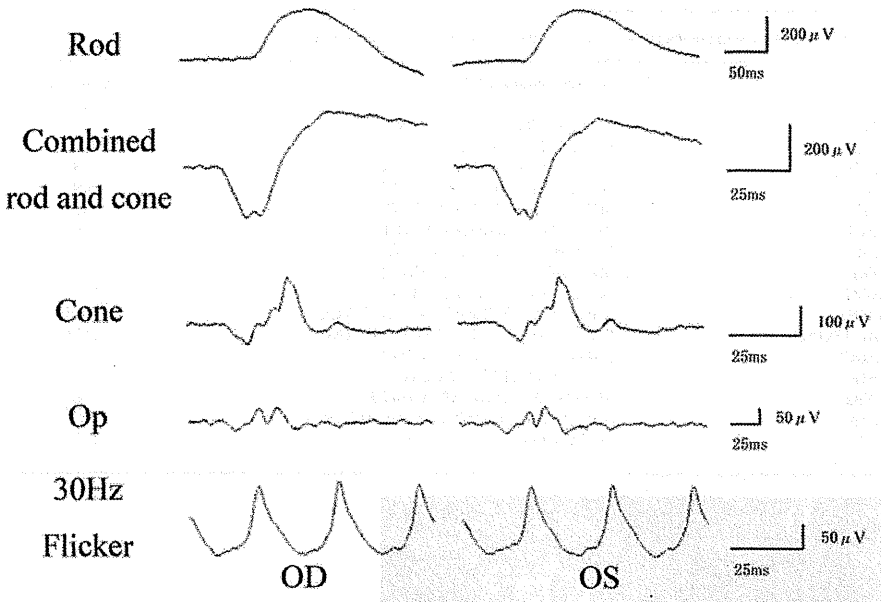

Figure 2. Full-field electroretinograms (ERGs) recorded according to the International Society for Clinical Electrophysiology of Vision (ISCEV) standards protocol in this case. The rod, combined rod-cone, cone, oscillatory potentials, and 30-Hz flicker full-field ERGs are shown. The results of full-field ERGs are within the normal limits in this case.

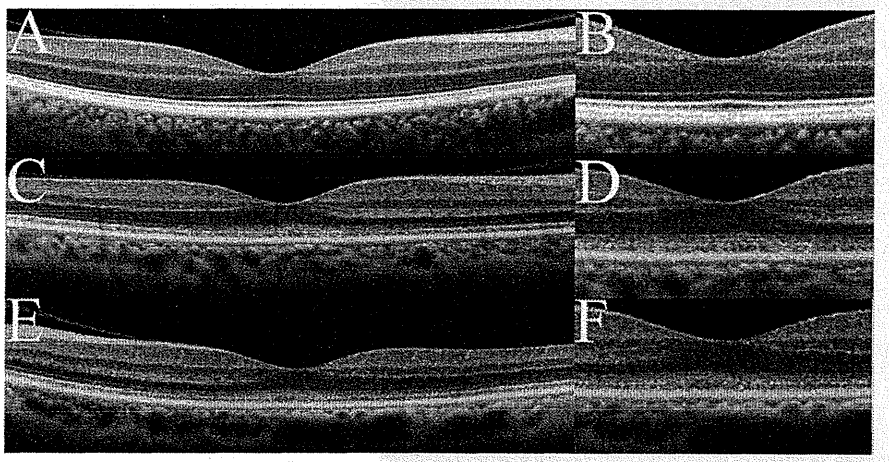

Figure 3. Spectral-domain optical coherence tomography (SD-OCT) findings of the eyes in normal controls (**A**, **B**) and in this case (**C-F**). Images from right eyes (**C**, **D**) and left eyes (**E**, **F**) are shown. Images at lower magnification (**A**, **C**, **E**) and higher magnification (**B**, **D**, **F**) are shown. The SD-OCT findings for the eyes in this case show obvious blurring of the IS/OS junction and the COST line. The COST line disappeared in the peripheral macula area in this case.

this control group. We recorded focal macular ERGs from either of the eyes of normal controls and calculated the 95% CI of the amplitudes of the a-waves and the b-waves, the implicit time of the a-waves and b-waves, the potentials at 70 ms after the stimulus was turned on, and the time of the recovery of the b-wave to the baseline.

RESULTS

Case report: A 52-year-old woman complained of a gradual decrease in vision in both eyes during the past two to three years. Family history revealed no other members with any eye diseases, including her parents who were deceased. Her BCVAs were 20/63 in the right eye and 20/50 in the left eye. The fundus examination, fluorescein angiography, and full-field ERG results were within the normal limits (Figure 1A-D and Figure 2). The visual fields were full with the Goldman perimetry, but a relative central scotoma was detected in both eyes with the Humphrey Visual Field Analyzer.

Spectral domain optical coherence tomography: The SD-OCT images of this case showed a blurred IS/OS junction and COST line at the foveal center (Figure 3D,F). In the peripheral macula area, the COST line was absent, and only the blurred IS/OS junction was visible in this case (Figure 3C,E).

Focal macular electroretinograms and multifocal electroretinograms: A severe reduction in the a-waves of the focal macular ERGs was found in this case (Figure 4). Although the b-waves were large, their shapes were abnormal. The b-waves rose to a peak, and the potential was maintained longer than normal. The plateau region of the b-wave was significantly elevated above the baseline potential (Figure 4,

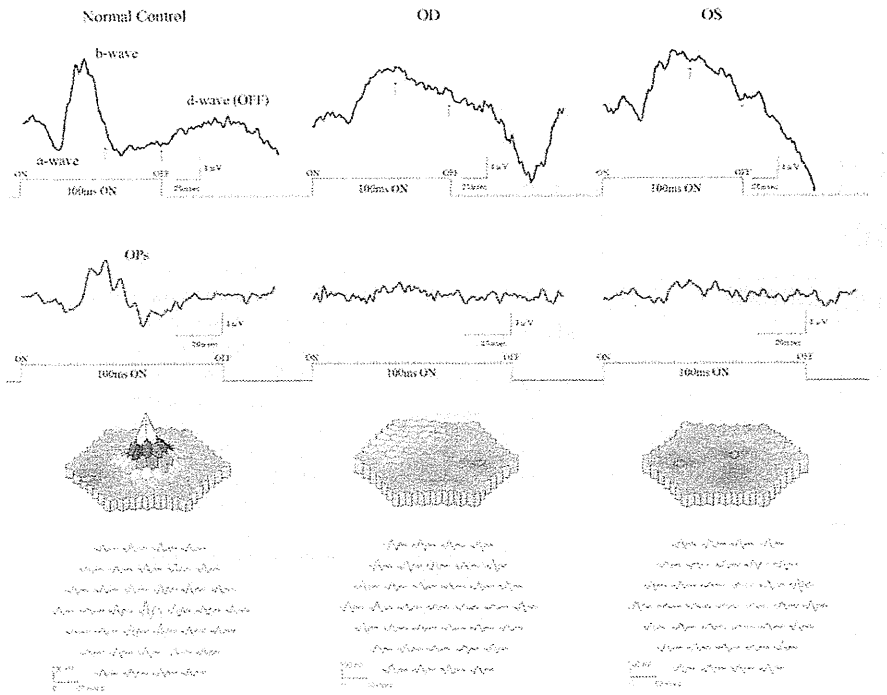

Figure 4. Results of focal macular electroretinograms (ERGs) and multifocal ERGs. Focal macular ERGs and oscillatory potentials recorded from a normal subject and this case are shown (top). The amplitude of the a-wave of this case was severely reduced, and the plateau region was significantly elevated (arrows). The topographic map and the local responses of multifocal ERGs recorded from the normal subject and this case are shown (bottom). The amplitudes in the foveal area were severely reduced in this case.

arrow). To analyze this characteristic, we quantified the potentials at 70 ms after the stimulus was turned on, and the recovery time of the descending slope of b-wave to the baseline from the peak of the b-wave. We calculated the 95% confidence intervals (CI) for the amplitudes of the a-waves and b-waves, the implicit times of the a-waves and b-waves, the potentials at 70 ms after the stimulus turns on, and the time of the recovery of the b-waves to the baseline obtained from the normal controls (Figure 5). Among these six parameters, the amplitudes of the a-waves, the implicit times of the b-waves, the potentials at 70 ms after the stimulus was turned on, and the time of the recovery of the descending slope of the b-wave to the baseline obtained from both eyes of this case were outside the range of the standard deviation and the 95% CI of the normal controls (Figure 5). Especially, the amplitudes of the a-waves, the potentials at 70 ms after the stimulus was turned on, and the time of the recovery of the descending slope of the b-wave to the baseline obtained from this case were severely affected. The amplitudes of the mfERGs in the foveal area were severely reduced in this case (Figure 4).

Molecular genetic findings: Mutation analysis of the *RP1L1* gene in this case showed three missense mutations. There was a c.2578 C>T in exon 4 with a substitution of tryptophan (TGG) for arginine (CGG) at amino acid position 860, a c. 3596 C>G in exon 4 with a substitution of cysteine (TGT) for serine (TCT) at amino acid position 1199, and a c. 4484 C>G in exon 4 with a substitution of arginine (CGC) for proline (CCC) at amino acid position 1495. The amino acid substitution at position 860 and 1495 has already been reported in the SNP database and is found in a high percentage of the normal population. A mutation at amino acid position 1199 has not been reported in the SNP database or in earlier reports (Figure 6A). The serine at position 1199 is well conserved among the RP1L1 family in other species (Figure 6B). This mutation was predicted to be probably damaging with a score of 0.999 by PolyPhen-2. The SIFT tool analysis revealed a score of 0 and predicted that the replaced amino acid is potentially damaging and would not be tolerated. PMut predicted that this mutation is pathological. Align GVGD predicted this mutation as class C65, which means it most likely interferes with the protein function. Out of five computational assessments, only MutationTaster predicted this mutation as a polymorphism. We confirmed that the mutation in this case was segregated with the disease in one affected member and one unaffected member of the family (Figure 6C). The unaffected member of the family in Case 1 underwent clinical examination, including BCVAs, slit-lamp biomicroscopy, fundus ophthalmoscopy, OCT, and focal ERGs. All examination findings were normal. This mutation was not present in 300 control alleles. This mutation p.S1199C has been registered in GenBank with accession number AB684329.

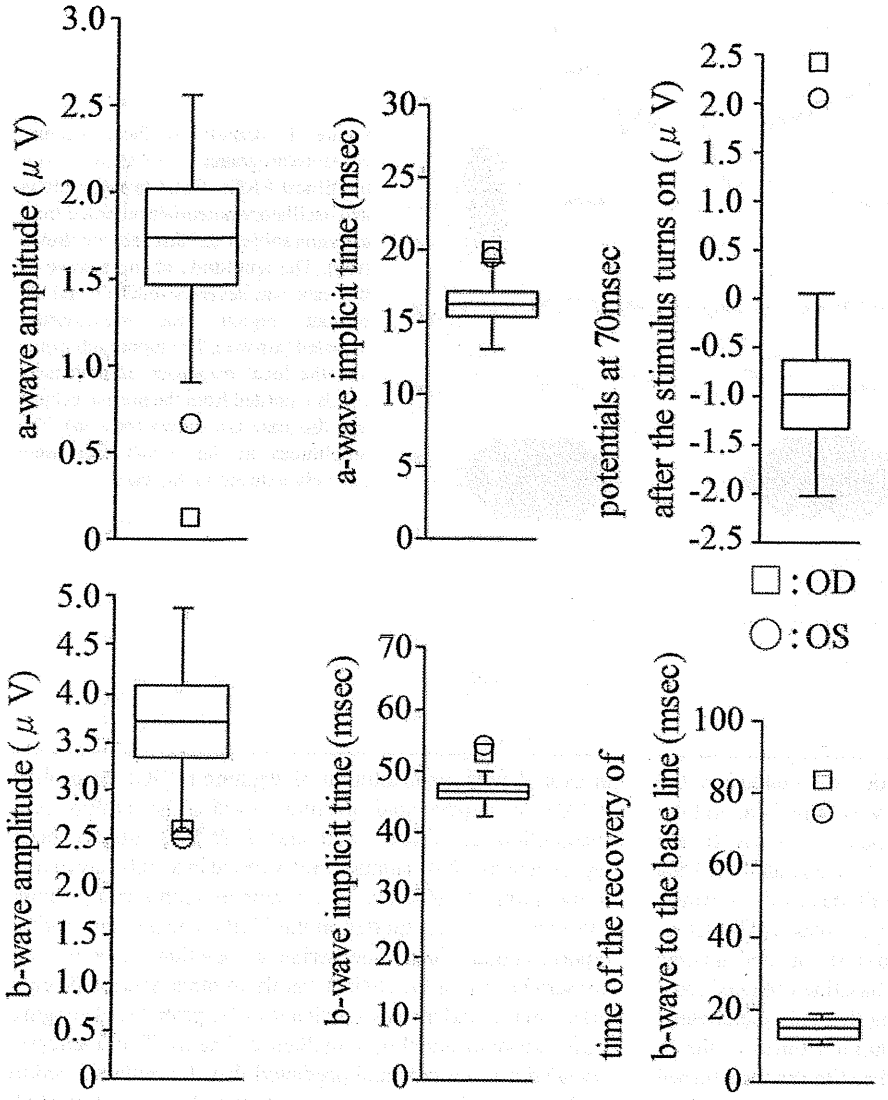

Figure 5. Plot of the amplitudes of the a-waves, b-waves, and the implicit time of the a-waves, b-waves, the potentials at 70ms after the stimulus turns on, and the time of the recovery of b-wave to the baseline for normal controls. There were 25 men and 21 women whose age ranged from 23 to 60 years (mean, 38.04±8.33 years) in this control group. The boxes represent the 95% confidence interval ranges, the horizontal line represents mean values, and the bars represent standard deviation. Data recorded from this case are plotted at indicated mark.

Bowne et al. [11] reported that *RP1L1* mRNA is variable due to the presence of a 48 bp polymorphic coding repeat. They reported that as many as six 48 bp repeats have been observed in normal controls. In this case, one allele contains a 48 bp repeat, and the other allele contains three 48 bp repeats (Figure 6D). There are variations of only two amino acids in the length polymorphism region from this case compared to the reference sequence (NP_849188). One variation with the substitution of E to G in the 14th amino acid of the length polymorphism region was in a previous report [12] (AAN86962, AAN86963, and AAN86964). The other variation with the substitution of G to V in the ninth amino acid of the length polymorphism region was found in more than 10 normal control alleles from a Japanese population. These variations of the length polymorphisms of *RP1L1* with one and three repeats have been registered in GenBank with accession numbers AB684331 and AB684332, respectively.

DISCUSSION

The mutation found in the *RP1L1* gene in this case was a missense mutation with cysteine substituted for serine at amino acid position 1199. This residue is well conserved among the RP1L1 family in other species, suggesting the importance of this amino acid residue for RP1L1 function. Four out of five computational analysis tools predicted this mutation is damaging to the protein function. We did not find this mutation in the sister of the patient with normal vision, although she was the only other family member we were able to test. To decide whether this mutation was pathogenic, we need to examine more family members and a larger number

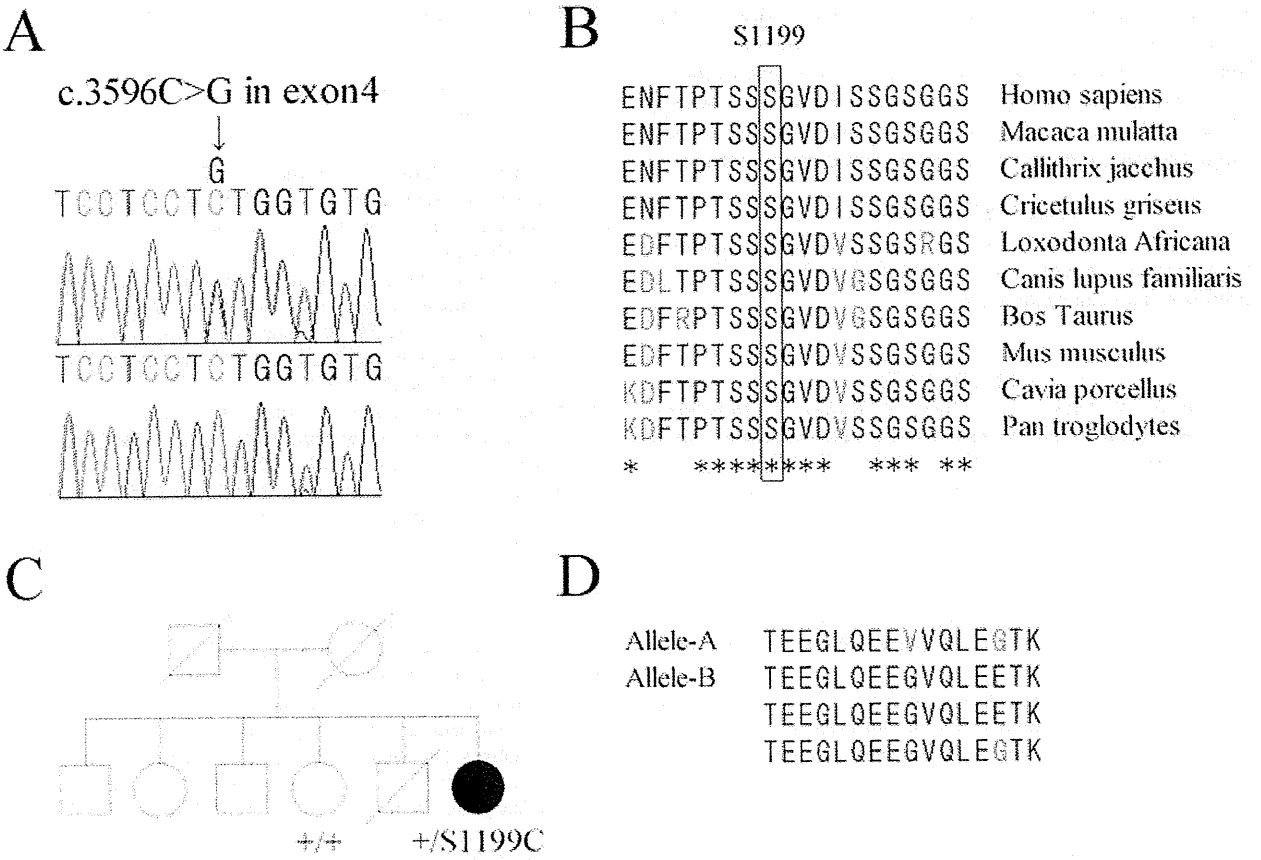

Figure 6. DNA analysis for c.3596C>G mutation and deduced amino acids of length polymorphism region of the RP1-like protein 1 (*RP1L1*) gene and the pedigree of the family with *RP1L1* gene mutation. **A**: Sequence chromatograms for this case (top) and the normal control (bottom) are shown. This case had a c.3596 C>G mutation in exon 4. **B**: Alignment of S1199 in the RP1L1 family proteins. Amino acid-sequence alignments of RP1L1 from 10 species reported in the NCBI database are shown. Amino acid residues of S1199 in humans and conserved residues from other species are boxed. The asterisks indicate completely conserved residues. S1199 is well conserved in all species reported. **C**: We confirmed that the mutation in Case 1 was segregated with the disease in one affected member and one unaffected member of the family. **D**: Deduced amino acids (AA) of repeated regions of the RP1L1 length polymorphism. In this case, one allele contains a 16 AA, and the other allele contains three 16 AA repeats. Variations of amino acids from reference sequence of RP1L1 are shown in red. Those variations are within normal limits.

of normal controls. However, the phenotype of this case was typical of OMD, and thus the mutation in this case was most likely pathogenic.

The photoreceptor IS/OS junction and the COST line can be detected in the SD-OCT images of normal eyes [25-28]. Recently, several degrees of disruption of the IS/OS junction and/or COST line in the SD-OCT images of patients with OMD have been reported [4-8]. In our case, the IS/OS junction and the COST line appeared blurred in the SD-OCT images similar to previous reports.

Researchers have emphasized that the key to differentiating OMD from other diseases, such as optic neuritis or psychological disorders, is the recording of focal macular ERGs from the central retina [1-3]. Focal macular ERGs have a unique waveform when elicited by long-duration stimuli [29]. As shown in this patient, the waveform of focal macular ERGs recorded from patients with OMD with long-duration stimuli had a depolarizing pattern, simulating the ERG waveforms observed after the hyperpolarizing bipolar cell activity is blocked [30-33]. Researchers have demonstrated that by blocking hyperpolarizing bipolar cells with cis-2,3-piperidine dicarboxylic acid or kynurenic acid in monkeys, the a- and d-waves of photopic ERGs become smaller and the plateau between the b- and d-waves remains elevated above the baseline potential [34]. Full-field cone ERG in some human retinal dystrophies show a similar depolarizing pattern [29,35]. Kondo et al. [29] reported similar focal macular ERGs elicited with 100 ms stimuli from a patient with glittering crystalline deposits in the posterior fundus. The waveform of the focal macular ERGs of this case

was similar to those reported for patients with OMD [31-33]. Because this case had a putative disease-causing mutation of the *RP1L1* gene, we suggest the reduced amplitude of the a-wave and the persistent plateau between the b- and d-waves of the focal macular ERGs elicited with long-duration stimuli might be specific markers that could help diagnose OMD.

ACKNOWLEDGMENTS

We thank Dr. Duco Hamasaki (Bascom Palmer Eye Institute, University of Miami School of Medicine, Miami, FL) for proofreading of our manuscript.

REFERENCES

1. Miyake Y, Ichikawa K, Shiose Y, Kawase Y. Hereditary macular dystrophy without visible fundus abnormality. Am J Ophthalmol 1989; 108:292-9. [PMID: 2774037]
2. Miyake Y, Horiguchi M, Tomita N, Kondo M, Tanikawa A, Takahashi H, Suzuki S, Terasaki H. Occult macular dystrophy. Am J Ophthalmol 1996; 122:644-53. [PMID: 8909203]
3. Matthews GP, Sandberg MA, Berson EL. Foveal cone electroretinograms in patients with central visual loss of unexplained etiology. Arch Ophthalmol 1992; 110:1568-70. [PMID: 1444913]
4. Park SJ, Woo SJ, Park KH, Hwang JM, Chung H. Morphologic photoreceptor abnormality in occult macular dystrophy on spectral-domain optical coherence tomography. Invest Ophthalmol Vis Sci 2010; 51:3673-9. [PMID: 20164460]
5. Sisk RA, Berrocal AM, Lam BL. Loss of Foveal Cone Photoreceptor Outer Segments in Occult Macular Dystrophy. Ophthalmic Surg Lasers Imaging 2010; 9:1-3. [PMID: 20337322]
6. Kim YG, Baek SH, Moon SW, Lee HK, Kim US. Analysis of spectral domain optical coherence tomography findings in occult macular dystrophy. Acta Ophthalmol 2011; 89:e52-6. [PMID: 20560888]
7. Fujinami K, Tsunoda K, Hanazono G, Shinoda K, Ohde H, Miyake Y. Fundus autofluorescence in autosomal dominant occult macular dystrophy. Arch Ophthalmol 2011; 129:597-602. [PMID: 21555613]
8. Tsunoda K, Usui T, Hatase T, Yamai S, Fujinami K, Hanazono G, Shinoda K, Ohde H, Akahori M, Iwata T, Myake Y. Clinical characteristics of occult macular dystrophy in family with mutation of RP1L1 gene. Retina. 2012 [PMID: 22466457]In press
9. Lyons JS. Non-familial occult macular dystrophy. Doc Ophthalmol 2005; 111:49-56. [PMID: 16502307]
10. Akahori M, Tsunoda K, Miyake Y, Fukuda Y, Ishiura H, Tsuji S, Usui T, Hatase T, Nakamura M, Ohde H, Itabashi T, Okamoto H, Takada Y, Iwata T. Dominant mutations in RP1L1 are responsible for occult macular dystrophy. Am J Hum Genet 2010; 87:424-9. [PMID: 20826268]
11. Conte I, Lestingi M, den Hollander A, Alfano G, Ziviello C, Pugliese M, Circolo D, Caccioppoli C, Ciccodicola A, Banfi S. Identification and characterization of the retinitis pigmentosa 1-like1 gene (RP1L1): a novel candidate for retinal degenerations. Eur J Hum Genet 2003; 11:155-62. [PMID: 12634863]
12. Bowne SJ, Daiger SP, Malone KA, Heckenlively JR, Kennan A, Humphries P, Hughbanks-Wheaton D, Birch DG, Liu Q, Pierce EA. Characterization of RP1L1, a highly polymorphic paralog of the retinitis pigmentosa 1 (RP1) gene. Mol Vis 2003; 9:129-37. [PMID: 12724644]
13. Yamashita T, Liu J, Gao J, LeNoue S, Wang C, Kaminoh J, Bowne SJ, Sullivan LS, Daiger SP, Zhang K. Essential and synergistic roles of RP1 and RP1L1 in rod photoreceptor axoneme and retinitis pigmentosa. J Neurosci 2009; 29:9748-60. [PMID: 19657028]
14. Marmor MF, Fulton AB, Holder GE, Miyake Y, Brigell M, Bach M, International Society for Clinical Electrophysiology of Vision. ISCEV Standard for full-field clinical electroretinography (2008 update). Doc Ophthalmol 2009; 118:69-77. [PMID: 19030905]
15. Miyake Y, Shiroyama N, Horiguchi M, Ota I. Asymmetry of focal ERG in human macular region. Invest Ophthalmol Vis Sci 1989; 30:1743-9. [PMID: 2759790]
16. Miyake Y. Macular oscillatory potentials in humans: macular OPs. Doc Ophthalmol 1990; 75:111-24. [PMID: 2276312]
17. Miyake Y. Focal macular electroretinography. Nagoya J Med Sci 1998; 61:79-84. [PMID: 9879190]
18. Bearse MA Jr, Sutter EE. Imaging localized retinal dysfunction with the multifocal electroretinogram. J Opt Soc Am A Opt Image Sci Vis 1996; 13:634-40. [PMID: 8627420]
19. Adzhubei IA, Schmidt S, Peshkin L, Ramensky VE, Gerasimova A, Bork P, Kondrashov AS, Sunyaev SR. A method and server for predicting damaging missense mutations. Nat Methods 2010; 7:248-9. [PMID: 20354512]
20. Ng PC, Henikoff S. SIFT. Predicting amino acid changes that affect protein function. Nucleic Acids Res 2003; 31:3812-4. [PMID: 12824425]
21. Ferrer-Costa C, Orozco M, de la Cruz X. Characterization of disease-associated single amino acid polymorphisms in terms of sequence and structure properties. J Mol Biol 2002; 315:771-86. [PMID: 11812146]
22. Tavtigian SV, Deffenbaugh AM, Yin L, Judkins T, Scholl T, Samollow PB, de Silva D, Zharkikh A, Thomas A. Comprehensive statistical study of 452 BRCA1 missense substitutions with classification of eight recurrent substitutions as neutral. J Med Genet 2006; 43:295-305. [PMID: 16014699]
23. Mathe E, Olivier M, Kato S, Ishioka C, Hainaut P, Tavtigian SV. Computational approaches for predicting the biological effect of p53 missense mutations: a comparison of three sequence analysis based methods. Nucleic Acids Res 2006; 34:1317-25. [PMID: 16522644]
24. Schwarz JM, Rödelsperger C, Schuelke M, Seelow D. MutationTaster evaluates disease-causing potential of sequence alterations. Nat Methods 2010; 7:575-6. [PMID: 20676075]
25. Srinivasan VJ, Monson BK, Wojtkowski M, Bilonick RA, Gorczynska I, Chen R, Duker JS, Schuman JS, Fujimoto JG. Characterization of outer retinal morphology with high-speed, ultrahigh-resolution optical coherence tomography. Invest Ophthalmol Vis Sci 2008; 49:1571-9. [PMID: 18385077]
26. Marmor MF, Choi SS, Zawadzki RJ, Werner JS. Visual insignificance of the foveal pit: reassessment of foveal

hypoplasia as fovea plana. Arch Ophthalmol 2008; 126:907-13. [PMID: 18625935]

27. Byeon SH, Kang SY. Interpretation of outer retina appearance in high-resolution optical coherence tomography. Am J Ophthalmol 2009; 147:185-6. [PMID: 19100358]
28. Lim JI, Tan O, Fawzi AA, Hopkins JJ, Gil-Flamer JH, Huang D. A pilot study of Fourier-domain optical coherence tomography of retinal dystrophy patients. Am J Ophthalmol 2008; 146:417-26. [PMID: 18635153]
29. Kondo M, Miyake Y. Assessment of local cone on- and off-pathway function using multifocal ERG technique. Doc Ophthalmol 2000; 100:139-54. [PMID: 11142743]
30. Miyake Y. What can we know from focal macular ERG? Jpn J Clin Ophthalmol. 2002; 56:680-8.
31. Okuno T, Oku H, Kondo M, Miyake Y, Sugasawa J, Utsumi T, Ikeda T. Abnormalities of visual-evoked potentials and pupillary light reflexes in a family with autosomal dominant occult macular dystrophy. Clin Experiment Ophthalmol 2007; 35:781-3. [PMID: 17997791]
32. Hanazono G, Ohde H, Shinoda K, Tsunoda K, Tsubota K, Miyake Y. Pattern-reversal visual-evoked potential in patients with occult macular dystrophy. Clin Ophthalmol. 2010; 4:1515-20. [PMID: 21191449]
33. Miyake Y. Occult macular dystrophy. Elctrodiagnosis of retinal diseases. Tokyo, Japan: springer-Verlag; 2006:153–159
34. Sieving PA, Murayama K, Naarendorp F. Push-pull model of the primate photopic electroretinogram: a role for hyperpolarizing neurons in shaping the b-wave. Vis Neurosci 1994; 11:519-32. [PMID: 8038126]
35. Sieving PA. 'Unilateral cone dystrophy': ERG changes implicate abnormal signaling by hyperpolarizing bipolar and/or horizontal cells. Trans Am Ophthalmol Soc 1994; 92:459-71. [PMID: 7886877]

Articles are provided courtesy of Emory University and the Zhongshan Ophthalmic Center, Sun Yat-sen University, P.R. China. The print version of this article was created on 20 April 2012. This reflects all typographical corrections and errata to the article through that date. Details of any changes may be found in the online version of the article.

ANTICANCER RESEARCH *31*: 2511-2516 (2011)

Novel Complementary Peptides to Target Molecules

HIDECHIKA OKADA[1], MASAKI IMAI[2], FUMIKO ONO[3], ALAN OKADA[1], TOYOHIRO TADA[4], YUKA MIZUE[5], KEIJI TERAO[3] and NORIKO OKADA[2]

[1]*Research Institute for Protein Science, Nakayama-cho 2-18, Mizuho-ku, Nagoya 467-0803, Japan;*
[2]*Nagoya City University Graduate School of Medical Sciences, Mizuho-cho, Mizuho-ku, Nagoya 467-8601, Japan;*
[3]*Tsukuba Primate Research Center, National Institute of Biomedical Innovation, Tsukuba 305-0843, Japan;*
[4]*Nagoya City University School of Nursing, Nagoya 467-8601, Japan;*
[5]*Sapporo Immuno Diagnostic Laboratory, Sapporo 001-0922, Japan*

Abstract. *We generated an evolutionary computer program that generates complementary peptide (C-pep) sequences, with the potential to interact with a target peptide, by comparing several physico-chemical parameters of each pair of the complementary peptides being analyzed. We generated C-peps to target several molecules. About 30% of synthesized C-peps interfered with the function of their targets. C5a stimulates generation of TNFα and other inflammatory cytokines. Inhibition of C5a should be effective against sepsis, which impairs the status of cancer-bearing patients. One of the inhibitory C-peps of C5a, termed AcPepA, was effective in Cynomolgus monkeys intravenously infused with a lethal dose of bacterial LPS (4 mg/kg) destined to die. The monkeys were rescued by intravenous administration of 2 mg/kg/h of AcPepA. The excellent therapeutic effect of AcPepA is likely to be due to restriction of high mobility group box 1 (HMGB1) surge induced by the effect of C5a on C5L2, which is the second C5a receptor, since the released HMGB1 has the capacity to stimulate TLR4 as an endogeneous ligand resulting in further activation of inflammatory cells to release inflammatory cytokines forming a positive feedback circuit of inflammation.*

After proposal of the possible role of antisense peptides for molecular interaction among proteins by Blalock *et al.* (1) in 1984, the theory was reviewed later (2, 3). Many examples of sense–peptide and antisense–peptide relationships have been found between receptors and their protein ligands (4-8). We speculated that such interactions between sense and antisense peptides should play a role in formation of the tertiary structure of proteins. We developed a novel computer program named ANTIS to find antisense peptide sequences between proteins to be compared (9). By analyzing intramolecular antisense peptides within a single protein molecule, we found that there are an appreciable number of sense and antisense peptide pairs within a protein molecule and we designated these as antisense homology boxes (AHB) (9). Using ANTIS, we analyzed sense and antisense peptide relationships in the endothelin receptor (ETR) molecule and between endothelin and ETR. One of the AHB peptides of ETR, named ETR-P1/fl, had the capacity to interfere with the function of ETR (10). We expected that it would be possible to generate candidates of complementary peptide reactive to a target amino acid sequence based upon the sense-antisense amino acid relationship. We generated an evolutionary computer program that runs on any PC, and generates complementary peptide (C-pep) sequences, with the potential to interact with a target peptide, by comparing several physico-chemical parameters of each pair of the complementary peptides being analyzed (11). With the program named MIMETIC, we generated complementary peptides (C-peps) to HIV-reverse transcriptase (11, 12), procarboxypeptidase R, thrombomodulin (13), and C5a anaphylatoxin (14) as listed in Table I. About 30% of the synthesized peptides interfered with the function of their target molecules. Out of 19 complementary peptides (C-peps) targeted to C5a anaphylatoxin, 7 exhibited an inhibitory effect.

C5a is a 74 amino acid peptide released from the fifth component of complement (C5) by C5 convertase generated during complement activation (15). C5a anaphylatoxin is considered to be an effective target for treatment of hyperinflammation since C5a stimulates generation of tumor necrosis factor alpha (TNFα) and other inflammatory cytokines (16-18). Although C5a generated *in vivo* is regulated by carboxypeptidase N and more efficiently by carboxypeptidase R (CPR) (19, 20), excessive generation of

Correspondence to: H. Okada, Research Institute for Protein Science, Nakayama-cho 2-18, Mizuho-ku, Nagoya 467-0803, Japan. Tel: +81 9027738012, Fax: +81 528535112, e-mail: hiokada@med.nagoya-cu.ac.jp

Key Words: Antisense pepitide, complementary peptide, anaphylatoxin, inflammation, sepsis, cytokine storm.

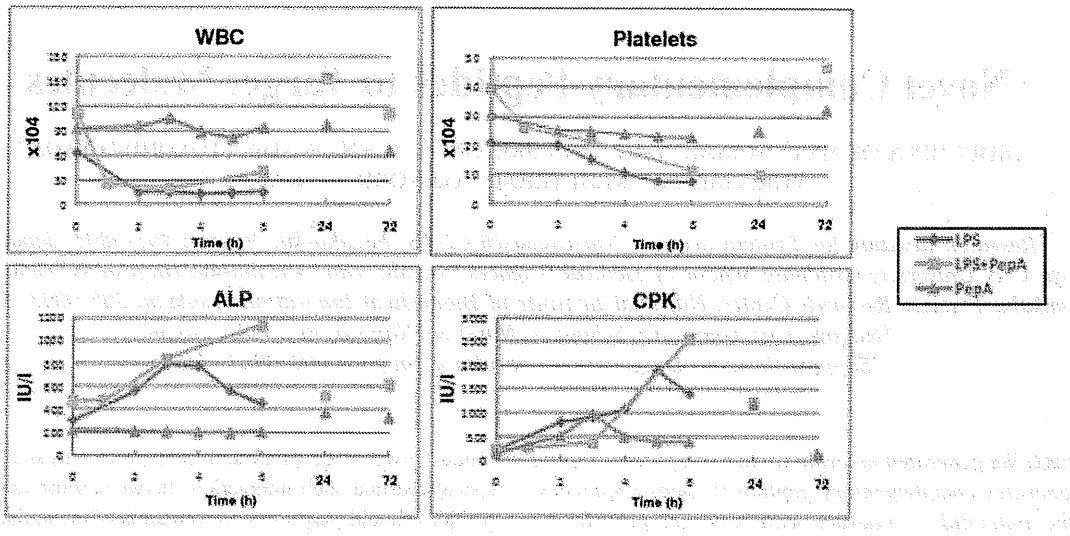

Figure 1. *Clinical features in peripheral blood of endotoxin-shocked monkeys. Extensive leukopenia (WBC), and thrombopenia (platelets), increased alkaline phosphatase (ALP), as well as increased creatinine phosphokinase (CPK), were observed in blood from AcPepA-treated monkeys and in untreated monkeys following LPS injection. Esssentially no significant changes were observed in a monkey treated with AcPepA alone without LPS injection.*

C5a appears to exceed the capacity of CPR, since administration of lipopolysaccharide (LPS) at a lethal dose to rats exhausted CPR capacity before death (21). However, attempts to restrict the effect of C5a with C5a receptor (C5aR) antagonists would not be successful because C5aR is not only expressed on inflammatory leukocytes, but also on many other cell types (17). Furthermore, C5aR numbers increase in an acute inflammatory state (22).

On the other hand, antibodies to C5a have been demonstrated to be effective in treating experimental primate models of sepsis (16, 23), indicating that C5a inhibitors should be useful for treatment of patients suffering from hyperinflammation such as in sepsis and multiple organ failure (24). If an inhibitor of C5a has a therapeutic effect on sepsis, which impairs the status of cancer-bearing patients, the inhibitor could be beneficial for the cancer patients in order to improve their performance status.

AHB in C5aR, and between C5aR and C5a were analyzed by ANTIS program, and we found that amino acids 37 to 53 of C5a (RAARISLGPRCIKAFTE) comprise an antisense peptide to AHB peptides (9) of the C5aR, and this has been designated PL37 (25). This region of C5a is presumed to be a potential site for C5aR stimulation (26). Using the computer program MIMETIC (11), we generated 19 C-peps to PL37. One of the 7 inhibitory C-peps to PL37 which interfered with C5a function was termed PepA (ASGAPAPGPAGPLRPMF) (14). To improve stability, we modified PepA by acetylation of its *N*-terminal alanine generating acetylated PepA (AcPepA) which was more stable in animal experiments (27). In preliminary experiments with human lung tissues, AcPepA successfully suppressed the allergic response *in vitro* (28). Therefore, we performed experiments in *Cynomolgus* monkeys *in lieu* of using humans.

Table I. *Inhibitory capacity of complementary peptides (C-pep) to target molecules. Complementary peptides designed by MIMETIC program were synthesized and their inhibitory capacity on the function of target molecules determined. About 30% of these peptides interfered with the activity of target molecules.*

Target molecule	Activity of target	Number of C-pep	
		Tested	Effective (%)
HIV-RT*	Enzyme activity	10	3 (30%)
ProCPR **(TAFI)	Enzyme activity	10	3 (30%)
Thrombomodulin	Cofactor activity***	3	2 (67%)
C5a anaphylatoxin	Bioactivity	19	7 (37%)

*RT: Reverse transcriptase (12); **ProCPR: procarboxypeptidase R; ***cofactor activity for thrombin (13).

Materials and Methods

Peptides. PepA (ASGAPAPGPAGPLRPMF) whose *N*-terminal alanine is acetylated (AcPepA) was synthesized and purified (over 95% purity) by Biologica Co. Ltd. (Nagoya, Japan). The peptide was dissolved in saline at a concentration of 2 mg/ml and passed through a 0.22 μm Millipore filter prior to administration intravenously with an automated injection pump.

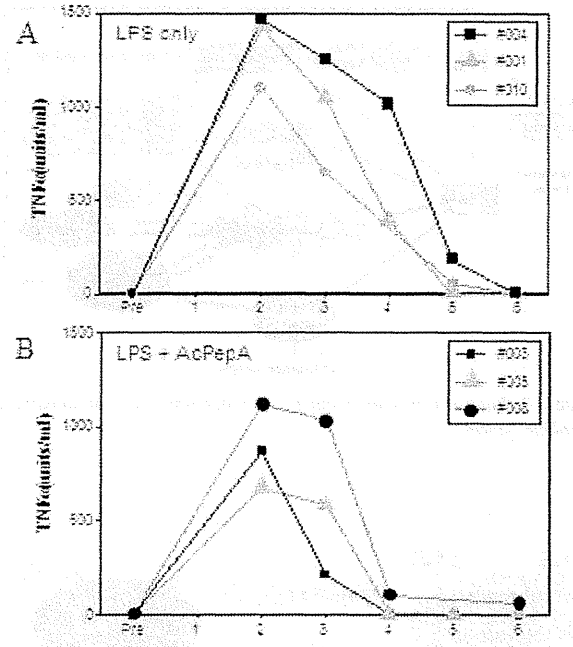

Figure 2. *TNFα levels in plasma of monkeys injected with 4 mg/kg LPS (A) and monkeys treated with AcPepA following the LPS injection (B). AcPepA i (2 mg/kg/h) was intravenously infused from 30 min to 6 h following LPS injection. AcPepA treatment suppressed the TNFα level to approximately 60% those of the untreated monkeys. TNFα in plasma disappeared within 4 h after LPS injection in AcPepA-treated monkeys, whereas this took 5 h in untreated monkeys.*

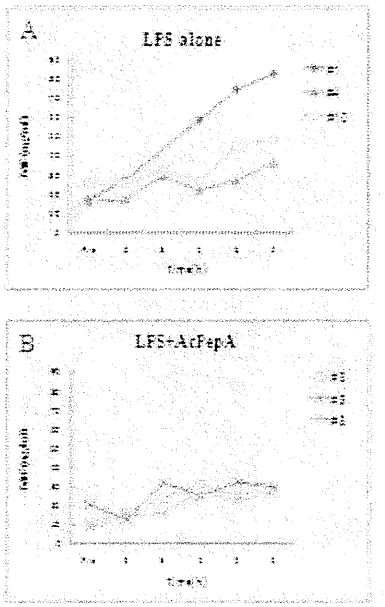

Figure 3. *Macrophage migration inhibitory factor (MIF) levels in plasma. Monkeys injected with LPS alone (#1, #4, #10; A), and monkeys treated with AcPepA following the LPS injection (#3, #5, #8; B) were tested for their MIF levels. MIF of AcPepA-treated monkeys remained at low levels (less than 30 ng/ml), whereas that of untreated monkeys increased to over 30 ng/ml following LPS injection.*

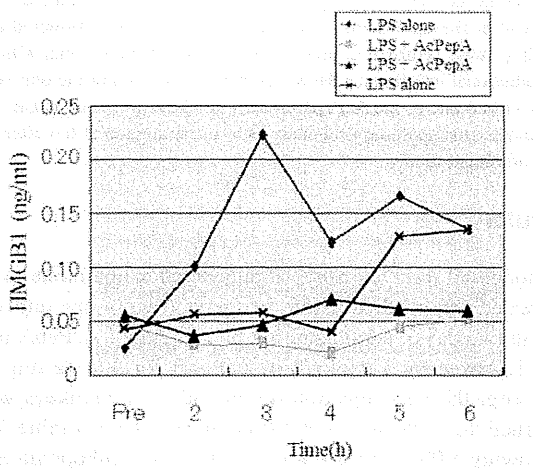

Figure 4. *Increase of HMGB1 in plasma of monkeys injected with LPS. Monkeys injected with LPS alone (#1, #10) showed increased HMGB1 levels in plasma, while AcPepA treatment following LPS injection (#5, #8) did not cause an increase (34).*

Monkeys. Cynomolgus monkeys were supplied from a breeding colony maintained at the Corporation for Production and Research of Laboratory Primates (CPRLP), Tsukuba, Japan. The Institutional Animal Ethical Committee of the Choju Medical Institute, Fukushimura Hospital, and the Institutional Animal Care Use Committees of the Tsukuba Primate Research Center, National Institute of Biomedical Innovation approved the study protocol. Animals weighed 4 to 5.5 kg, had hematocrits exceeding 36% and were free of infection, including tuberculosis. Animals were held for one month prior to LPS-lethal shock studies at CPRLP.

Titration of cytokine levels in plasma. TNFα in monkey plasma was determined using an ELISA kit purchased from Quantikine Immunoassay (Minneapolis, MN, USA). Macrophage inhibitory factor (MIF) was determined by use of an ELISA kit (29) prepared by Sapporo Immuno Diagnostic Laboratory (Sapporo, Japan). For high mobility group box 1 (HMGB1) determination, an ELISA kit from Shino-Test Co. (Sagamihara-shi, Kanagawa, Japan) was used.

Treatment of Cynomolgus monkeys. Fourteen monkeys were used for the experiment, and 13 were administered a lethal dose of LPS (4 mg/kg) sufficient to kill a monkey within 2 days, and 1 monkey was not administered LPS as an untreated control. Following sedation using ketamine hydrochloride (14 mg/kg, subcutaneously), monkeys were anesthetized with sodium pentobarbital administered through the capalic vein *via* a percutaneous catheter to maintain light surgical anesthesia. Oral intubation allowed animals to breathe spontaneously. Under anesthesia with sodium pentobarbital, 13 monkeys were intravenously administered 4 mg/kg LPS within 30 min. Thirty minutes after the LPS injection, 8 of the 14 animals were

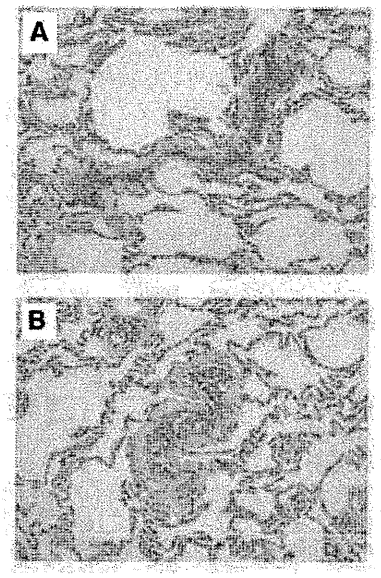

Figure 5. *Inflammation in lungs of monkeys 6 h after injection of a lethal dose of LPS observed in AcPepA-treated monkey (B) was to the same extent as that in untreated monkeys after LPS injection (A). (Magnification: ×200).*

administered 2 mg/kg of AcPepA in 2 min followed by 2 mg/kg/h of AcPepA for 3 h. The other 6 LPS-injected monkeys were injected with saline instead of AcPepA treatment as untreated controls. Six hours after the LPS administration, anesthesia was terminated and monkeys were returned to their cages to observe their status without any additional interference. However, half (3 animals) of the untreated controls and one of the AcPepA-treated monkeys were euthanized for autopsy for histopathological analysis of inflammation at 6 h after the LPS administration.

Results

Although all three monkeys administered saline alone as an untreated control died within two days (two in one day and one in two days), administration of 2 mg/kg of AcPepA in 2 min followed by 2 mg/kg/h of AcPepA for 3 h starting 30 min after the LPS injection rescued all of 7 monkeys who returned to a healthy condition in two days (Table II). Following LPS administration, significant leukopenia and thrombopenia were observed in peripheral blood obtained 6 h after the LPS injection both from monkeys treated with AcPepA and from control monkeys treated with saline instead of AcPepA (Figure 1). The increased TNFα level in plasma obtained during experiments in AcPepA-treated monkeys was lowered by only about 30% compared with that of untreated monkeys (Figure 2). The increase in the level of MIF (Figure 3) and HMGB1 (Figure 4) after LPS injection tended to be suppressed in the AcPepA-treated monkeys. Some of the monkeys were sacrificed under

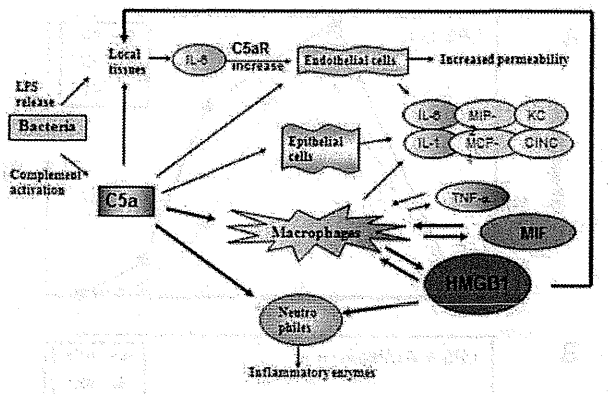

Figure 6. *Role of C5a anaphylatoxin in induction of an inflammatory cytokine 'storm'.*

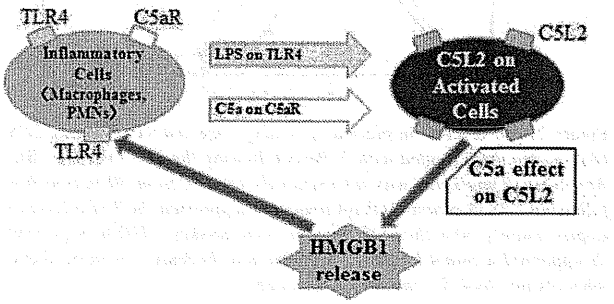

Figure 7. *Possible role for C5a in a positive feedback inflammatory circuit. Following bacterial infection, LPS stimulates TLR4, and C5a generated during complement activation stimulates C5aR, resulting in expression of C5L2 on leukocyte membranes. Stimulation of C5L2 by C5a on activated leukocytes induces release of HMGB1 which then reacts with TLR-4 on other leukocytes, as did LPS, resulting in further recruitment of activated leukocytes that express C5L2. These reactions create an inflammatory amplification circuit (34).*

anesthesia 6 h after LPS administration in order to perform autopsies. Pathological analysis of organ tissues showed serious inflammatory changes, including leukocyte infiltration, to the same extent in the lungs of both treated and untreated monkeys (Figure 5).

Discussion

The monkeys treated with AcPepA might have escaped induction of a feedback inflammatory circuit which was progressing gradually in LPS-treated monkeys at a late stage of the endotoxin shock syndrome as a vicious circle (Figure 6). This may be because HMGB1 has the capacity to stimulate toll-like receptor 4 (TLR4) and TLR2 as an endogenous stimulator (30, 31).

Table II. *Therapeutic effect of AcPepA on monkeys inoculated with a lethal dose of lipopolysaccharide (LPS) (4 mg/kg).*

	LPS alone	LPS and AcPepA	AcPepA alone
Decreased blood pressure	4/6	3/7	0/1
Increase in body temperature	5/6	3/7	0/1
Leukopenia	6/6	7/7	0/1
Increased CPK	6/6	7/7	0/1
Death	3/3	0/7	0/1
Euthanized at 6 h*	3	1	

CPK: Creatinine phosphokinase; *for histopathological analysis.

Consequently, inhibition of HMGB1 release presumably rescued animals suffering from septic vicious circle (32, 33). Therefore, suppression of HMGB1 in monkeys treated with AcPepA (Figure 4) could explain the extreme therapeutic effect of AcPepA on endotoxin shock in these animals (34). In other words, continuous generation of C5a by LPS or bacteria in monkeys receiving as well as possibly in patients with sepsis likely induce a cytokine 'storm' amplified by the release of HMGB1, resulting in a lethal effect on the host as a vicious circle of inflammation. The suppression of HMGB1 induction by inactivation of C5a could directly correlate with the survival observed following AcPepA treatment of monkeys injected with a lethal dose of LPS. Furthermore, AcPepA was shown to suppress pathophysiological events and prolonged survival time of piglets with sepsis induced by cecal ligation and perforation (CLP) (35, 36). Survival times were longer in the AcPepA-treated group than in the group treated with CLP alone (19.3 h±2.7 h *vs.* 9.9 h±0.7 h, $p<0.005$). In this case, AcPepA also delayed the HMGB-1 surge (36).

Therefore, suppression of C5 anaphylatoxin by AcPepA interferes with the induction of a cytokine 'storm'. Since C5a has the capacity to cause release of HMGB1 following stimulation of the second C5a receptor, termed C5L2, generated on activated monocytes (37-39), inhibition of C5a successfully interferes with the above release (Figure 7) (34).

Therefore, AcPepA would be beneficial for treatment of patients with sepsis and could be administered in large amounts at an acute stage, with little likelihood of an overdose, since the half-life of AcPepA in rats is 2.5 min. Administration of AcPepA to cancer patients at their terminal stage of their disease could improve their performance status.

Acknowledgements

This work was supported in part by a Research Grant from the Japanese Ministry of Health, Welfare and Labor (08062893).

References

1 Blalock J E and Smith EM: Hydropathic anti-complementarity of amino acids based on the genetic code. Biochem Biophys Res Comm *121*: 203-207, 1984.
2 Blalock JE: Complementarity of peptides specified by 'sense' and 'antisense' strands of DNA. Trends Biotech *6*: 140-144, 1991.
3 Trospha A, Kizer JS and Chaiken IM: Making sense from antisense: A review of experimental data and developing ideas on sense-antisense peptide recognition. J Molec Recognition *5*: 43-53, 1992.
4 Eberle AN and Huber MJ: Antisense peptides: Tools for receptor isolation? Lack of antisense MSH and ATH to interact with their sense peptides and induce receptor specific antibodies. Receptor Res *11*: 13-43, 1991.
5 Rassmundsen UB and Hesh RD: Antisense peptides: the parathyroid hormone as an experimental example and a critical theoretical view. Biochem Biophys Res Comm *149*: 930-938, 1987.
6 Goldstein A and Brutlag DL: Is there a relationship between DNA sequences encoding peptide ligands and their receptors? Proc National Acad Sci USA *86*: 42-45, 1989.
7 Guillemette G, Boulay G, Gagnon S, Bosse R and Escher E: The peptide encoded by angiotensin II complementary RNA does not interfere with angiotensin II action. Biochem J *261*: 309, 1989.
8 de Gasparo M, Whitebread S, Einsle K and Heusse C: Are the antibodies to a peptide complementary to angiotensin II useful to isolate angiotensin II receptor? Biochem J *261*: 310-311, 1989.
9 Baranyi L, Campbell W, Ohshima. K, Fujimoto S, Boros M and Okada H: The antisense homology box: a new motif within proteins that encodes biologically active peptides. Nature Med. *1*: 894-901, 1995.
10 Baranyi L, Campbell W, Oshima K, Fujimoto S, Boros M, Kaszaki J and Okada H. Antisense homology box-derived peptides represent a new class of endothelin receptor inhibitors. Peptides *19*: 211-223, 1998.
11 Campbell W, Kleiman L, Baranyi L, Khorchid Z, Li A, Fujita E, Okada N and Okada H: A novel genetic algorithm for designing mimetic peptides that interfere with the function of a target molecule. Microbiol Immunol *46*: 211-215, 2002.
12 Hosokawa M, Imai M, Okada H and Okada N: Inhibition of HIV-1 infection in cells expressing an artificial complementary peptide. Biochem Biophys Res Comm *324*: 236-240, 2004.
13 Shimomura Y, Kawamura T, Komura H, Campbell W, Okada N and Okada H: Modulation of procarboxypeptidase R (proCPR) activation by complementary peptides to thrombomodulin. Microbiol Immunol *47*: 241-245, 2003.
14 Fujita E, Farkas I, Campbell W, Baranyi L, Okada H and Okada N: Inactivation of C5a anaphylatoxin by a peptide that is complementary to a region of C5a. J. Immunol *172*: 6382-6387, 2004.
15 Ember JA and Hugli TE: Complement factors and their receptors Immunopharmacology *38*: 3-15, 1997.
16 Czermak BJ, Sarma V, Pierson CL, Warner RL, Huber-Lang M, Bless N.M, Schmal H, Friedl HP and Ward PA: Protective effects of C5a blockade in sepsis. Nature Med *5*: 788-792, 1999.
17 Guo RF and Ward PA: Role of C5a in inflammatory responses. Annu Rev Immunol *23*. 821-852, 2005.

18 Michael K: Targeting complement in therapy. Immunol Rev *180*: 177-189, 2001.
19 Campbell W, Lazoura E, Okada N and Okada H: Inactivation of C3a and C5a octapeptides by carboxypeptidase R and carboxypeptidase N. Microbiol Immunol *46*: 131-134, 2002.
20 Campbell W, Okada N and Okada H: Carboxypeptidase R (CPR) is an inactivator of complement derived inflammatory peptides and an inhibitor of fibrinolysis. Immunol Rev *180*: 162-167, 2001.
21 Kato K, Shinagawa N, Hayakawa T., Takeyama H, Campbell W and Okada H: Changes in arginine carboxypeptidase (CPR) activity in stressed rats. Pathophysiology *1*: 131-136, 1994.
22 Riedemann NC, Guo RF, Neff TA, Laudes IJ, Keller KA, Sarma VJ, Markiweski MM, Mastellos D, Strey CW, Pierson CL, Lambris JD, Zetoune FS and Ward PA: Increased C5a receptor expression in sepsis. J Clin Invest *110*: 101-108, 2002.
23 Stevens JH, O'Hanley P, Shapiro JM, Mihm FG, Satoh PS, Collins JA and Raffin TA: Effects of anti-C5a antibodies on the adult respiratory distress syndrome in septic primates. J Clin Invest *77*: 1812-1816, 1986.
24 Riedemann NC, Guo RF and Ward PA: Novel strategies for the treatment of sepsis. Nature Med *9*: 517-524, 2003.
25 Baranyi L, Campbell W and Okada H: Antisense homology boxes in C5a receptor and C5a anaphylatoxin. J Immunol *157*: 4591-4601, 1996.
26 Farkas I, Baranyi L, Liposits ZS, Yamamoto T and Okada H: Complement C5a anaphylatoxin fragment causes apoptosis in TGW neuroblastoma cells. Neuroscience *86*: 903-911, 1998.
27 Okada N, Asai S, Hotta A, Miura N, Ohno N, Farkas I, Hau L and Okada H: Increased inhibitory capacity of an anti-C5a complementary peptide following acetylation of *N*-terminal alanine. Microbiol Immunol *51*: 439-443, 2007.
28 Abe M, Hama H, Shirakusa T, Iwasaki A, Ono N, Kimura N, Hugli TE, Okada N, Katsuragi T and Okada H: Contribution of anaphylatoxins to allergic inflammation in human lungs. Microbiol. Immunol *49*: 981-986, 2005.
29 MizueY, Nishihira J, Miyazaki T, Fujiwara S, Chida M, NakamuraK, Kikuchi K and Mikai M: Quantitation of macrophage migration inhibitory factor (MIF) using the one-step sandwich enzyme immunosorbent assay: elevated serum MIF concentrations in patients with autoimmune diseases and identification of MIF in erythrocytes. Int J Mol Med *5*: 397-403, 2000.
30 Park JS, Gamboni-Robertson F, He Q, Svetkauskaite D, Kim JY, Strassheim D, Sohn JW, Yamada S, Maruyama I, Banerjee A, Ishizaka A and Abraham E: High mobility group box 1 protein interacts with multiple Toll-like receptors. Am J Physiol Cell Physiol *290*: C917-924, 2006.
31 Yu M, Wang H, Ding A, Golenbock DT, Latz E, Czura CJ, Fenton MJ, Tracey KJ and Yang H: HMGB1 signals through toll-like receptor (TLR) 4 and TLR2. Shock 26: 174-179, 2006.
32 Wang H, Bloom O, Zhang M, Vishnubhakat JM, Ombrellino M, Che J, Frazier A, Yang H, Ivanova S, Borovikova L, Manogue KR, Faist E, Abraham E, Andersson J, Andersson U, Molina PE, Abumrad NN, Sama A and Tracey KJ: HMGB-1 as a late mediator of endotoxin lethality in mice. Science *285*: 248-251, 1999.
33 Yang H, Ochani M, Li J, Qiang X, Tanovic M, Harris H, Susaria SM, Ulloa MP, Wang H, DiRimo R, Czura CJ, Wang H, Roth J, Warren HS, Fink MP, Fenton MJ, Andersson U and Tracey KJ. Reversing established sepsis with antagonists of endogeneous high-mobility group box 1. Proc Natl Acad Sci *101*: 296-301, 2004.
34 Okada N, Imai M, Okada A, Ono F and Okada H: HMGB1 release by C5a anaphylatoxin is an effective target for sepsis treatment. Nature Precedings, (hdl:10101/npre.2011.5727.1: Posted 23 Feb 2011) 2011.
35 Hussein MH, Kato S, Goto T, Daoud GA, Kato I, Suzuki S, Togari H, Imai M, Okada N and Okada H: An acetylated anti-C5a complementary peptide reduced cytokines and free radicals and prolongs survival time in a neonatal sepsis model Mol Immunol *46*: 2825, 2009.
36 Hussein MH, Daoud G Al-H, Goto T, Kato S, Nobata M, Kakita H, Mizuno H, Ito T, Kato I, Suzuki S, Okada N, Hashimoto T, Okada H and Togari H: An acetylated anti-C5a complementary peptide reduced cytokines and free radicals and prolonged survival time in a neonatal sepsis model. Critical Care Medicine, Submitted, 2011.
37 Chen NJ, Mirtsos C, Suh D, Lu YC, Lin WJ, McKerlie C, Lee T, Baribault H, Tian H and Yeh WC: C5L2 is critical for the biological activities of the anaphylatoxins C5a and C3a. Nature *446*: 203-207, 2007.
38 Klune JR, Dhupar R, Cardinal J, Billiar TR and Tsung A: HMGB1: Endogeneous danger signaling. Mol Med *14*: 476-484, 2008.
39 Rittirsch D, Flierl MA, Nadeau BA, Day DE, Huber-Lang M, Mackay CR, Zetoune FS, Gerard NP, Cianflone K, Koehl J, Gerard C, Sarma JV and Ward PA: Functional roles for C5a receptors in sepsis. Nature Med *14*: 551-557, 2008.

Received April 7, 2011
Revised June 8, 2011
Accepted June 9, 2011

J Gastroenterol
DOI 10.1007/s00535-011-0507-6

ORIGINAL ARTICLE—LIVER, PANCREAS, AND BILIARY TRACT

Targeting the hedgehog signaling pathway with interacting peptides to Patched-1

Masafumi Nakamura · Haruo Tanaka · Yousuke Nagayoshi · Hiroshi Nakashima · Kosuke Tsutsumi · Takao Ohtsuka · Shunichi Takahata · Masao Tanaka · Hidechika Okada

Received: 21 September 2011 / Accepted: 27 October 2011

Abstract
Background The hedgehog (Hh) signaling pathway is aberrantly activated in many cancers. Overproduction of sonic hedgehog (Shh), a ligand in the Hh pathway, increases Hh signaling activity by inhibiting Patched-1 (Ptch1), a suppressive receptor in the Hh pathway. The purpose of this study was to establish a novel strategy for treating pancreatic cancer and other Hh-dependent cancers through control of the tumor-suppressive function of Ptch1.
Methods We synthesized seven interacting peptides to the amino-acid sequence of the Ptch1 docking site for Shh. Human pancreatic cancer cell lines (AsPC-1, SUIT2) were cultured in the presence or absence of the peptides. Cell proliferation was assessed by cell counting and by the 3-(4,5-dimethylthiazol-2-yl)-2,5-diphenyltetrazolium bromide (MTT) assay. The activity of the Hh pathway was estimated by real-time polymerase chain reaction of the target gene product Gli1. To confirm their anti-tumor activity in vivo, the effect of the peptides in a mouse model of pancreatic cancer was determined. Finally, the Hh signaling activity of the xenograft was examined.
Results Three of the interacting peptides to Ptch1 suppressed the proliferation of the two pancreatic cancer cell lines and decreased the expression of Gli1, both in vitro and in vivo.
Conclusions This study suggests that interacting peptides to Ptch1 may be a new tool for controlling the Hh-dependent growth of pancreatic cancer.

Keywords Pancreatic cancer · Patched 1 protein · Peptides · Signal transduction

M. Nakamura and H. Tanaka contributed equally to this work.

M. Nakamura (✉) · H. Nakashima · K. Tsutsumi
Department of Digestive Surgery, Kawasaki Medical School, 577 Matsushima, Kurashiki 701-0192, Japan
e-mail: mnakamura@med.kawasaki-m.ac.jp

H. Tanaka · Y. Nagayoshi · T. Ohtsuka · S. Takahata · M. Tanaka
Department of Surgery and Oncology, Graduate School of Medicine, Kyushu University, Fukuoka, Japan

H. Okada
Research Institute for Protein Science, Nagoya, Japan

Introduction

Pancreatic cancer is one of the most lethal of all malignancies. The therapeutic options for patients with unresectable, metastatic, or recurrent disease are extremely limited, and few of these patients survive for 5 years [1]. Recently, gemcitabine and S1 have become available for these patients; however, although the prognosis of pancreatic cancer patients has improved slightly, it still remains poor [2, 3]. Thus, the development of novel therapeutics for pancreatic cancer is urgently required.

Recently, several molecular targeting drugs have been developed and some are now clinically available. However, these drugs generally target growth factor receptors or components of the signaling pathway connecting growth factors and Ras, a small GTP-binding protein. KRAS encodes Ras, which mediates the signaling pathway between extracellular growth-factor stimulation and cell-cycle activation [4]. Unfortunately, more than 90% of pancreatic cancers carry mutations in the KRAS oncogene. This is the highest proportion of KRAS alterations found in any human tumor type [5]. Mutated KRAS gene products constitutively activate Ras protein, resulting in the

Published online: 15 December 2011

constitutive activation of downstream pathways [5]. From the viewpoint of Ras mutation, the current development of molecular targeting drugs has still not been of major benefit to pancreatic cancer patients.

The hedgehog (Hh) signaling pathway has a crucial role in embryonic development, tissue regeneration, and carcinogenesis [6]. Recently, the Hh signaling pathway has been reported to be aberrantly activated in pancreatic cancer, in a ligand-dependent manner [6–12]. Without ligand stimulation, the transmembrane protein Patched-1 (Ptch1) suppresses another transmembrane protein Smoothened (Smo), which is the activator of the Hh signaling pathway. The Hh signaling pathway has three kind of ligands, Sonic Hh (Shh), Desert Hh (Dhh), and Indian Hh (Ihh). In pancreatic cancer cells, aberrantly overproduced Shh binds to Ptch1 and activates Smo, resulting in the translocation of Gli (glioma-associated oncogene) from the cytoplasm to the nucleus. Gli1, one of the three transactivators of the Hh signaling pathway, allows transcription of target genes of the Hh signaling pathway, including Gli1 itself. Thus, Gli1 is frequently used as a marker of activation of the Hh signaling pathway [13].

Suppression of the activated Hh signaling pathway is effective in controlling the development of many cancers in experimental studies [6–8, 12, 14, 15]. However, to date no drug has been developed to control the Hh signaling pathway and suppress cancer growth at the clinical level. We previously reported that anti-Ptch1 polyclonal antibodies raised against the docking site of Shh suppressed both Hh signaling activity and cancer cell growth [13]. However, polyclonal antibodies are far from being used clinically, and the generation of hybrid antibodies is costly.

We have developed an evolutionary computer program named MIMETIC that generates interacting peptide sequences, with the potential to interact with a target peptide. Thus, we have generated interacting peptides to HIV-reverse transcriptase [16, 17], procarboxypeptidase R, thrombomodulin [18], and C5a anaphylatoxin [19]. About 30% of the synthesized peptides interfered with the function of their target molecules [20]. In this study, we set out to generate synthetic interacting peptides to the short amino acid sequence of Ptch1, for which we had already raised antibodies [13], and we investigated the anti-cancer effect of these peptides in vitro and in vivo.

Materials and methods

Design and synthesis of interacting peptides to Ptch1

The target amino acid sequence of Ptch1 was selected according to our previous study [13]. Interacting peptides to the target sequences of Ptch1 were designed by the Institute for Protein Science (Nagoya, Japan), according to the method reported previously [16, 21]. Briefly, we used the MIMETIC program to design peptides that would interact with a target amino acid. This software employs a genetic algorithm that generates a series of increasingly optimized peptides to a target by random alteration of amino acids for 5,000 generations. Every peptide sequence generated in this manner is assigned a score based on several physico-chemical parameters, including hydropathic complementarity optimization, average structural similarity optimization, minimization of bulky side chain interference, and backbone alignment. Following the final generation, the program re-arranges the peptides into a list according to a scoring method for "goodness of fit" to the target. Eventually, seven peptides with high scores were selected, and the selected peptides were synthesized by Sigma-Aldrich Japan (Tokyo, Japan).

Cells and cell culture conditions

The human pancreatic cancer cell lines, AsPC1 and SUIT2, were maintained at 37°C under a humidified atmosphere of 5% CO_2 and 95% air in RPMI1640 medium (Life Technologies, Grand Island, NY, USA) supplemented with 10% fetal bovine serum (FBS; Life Technologies) and antibiotics (100 units/mL penicillin and 100 μg/mL streptomycin; Meijiseika, Tokyo, Japan) [4, 6].

Proliferation assay

The pancreatic cancer cell lines, AsPC1 and SUIT2, were seeded in 24-well plates at a concentration of 1×10^4 cells per well for cell counting with a Coulter counter (Beckman Coulter, Fullerton, CA, USA), and in 96-well plates at a concentration of 3×10^3 cells per well for the 3-(4,5-dimethylthiazol-2-yl)-2,5-diphenyltetrazolium bromide (MTT) assay, in complete culture medium. After overnight incubation, the medium was changed to fresh medium containing various concentrations of peptides for the MTT assay or 10 μg/mL of peptides for cell counting. Cells were incubated for 72 h (MTT assay), or for 48 and 72 h (cell counting). Then, cells were harvested by trypsin and viable cells were subjected to the MTT assay or cell counting using a Coulter counter [9].

Real-time reverse transcription-polymerase chain reaction (RT-PCR)

Total RNA was extracted using the RNeasy mini kit (Qiagen, Valencia, CA, USA) and quantified by spectrophotometry (Ultrospec 2100 Pro; Amersham Pharmacia Biotech, Cambridge, UK). RNA (700 ng) was treated with DNase, and reverse transcribed to cDNA using the Quantitect Reverse Transcription Kit (Qiagen) according to the

manufacturer's protocol. Reactions were run with SYBR Premix Ex Taq (Takara Bio, Otsu, Japan) on a DNA Engine Opticon 2 System (MJ Research, Waltham, MA, USA). pGli1-GFP (green fluorescent protein) was serially diluted in 10-fold increments and amplified with the primer pairs to generate a standard curve for Gli1. Each sample was run in triplicate. All primer sets amplified fragments that were 200 base pairs long. The sequences of the primers used were as follows: beta-actin, forward, 50-TTG CCG ACA GGA TGC AGA AGG A-30, reverse, 50-AGG TGG ACA GCG AGG CCA GGA T-30; and Gli1, forward, 50-GGT TCA AGA GCC TGG GCT GTG T-30, reverse, 50-GGC AGC ATT CTC AGT GAT GCT G-30. The quantity of gene in a given sample was normalized to the level of β-actin in that sample [12].

Table 1 Sequences of interacting peptides to Patched-1 (Ptch1)

Peptide	Sequence	Length
A	GAPGRPAGGGRRRRTG GLRRAAAPDRDY	28 mer
B	DNTRYSPPPPYSSHS	15 mer
C	DTLSCQSPESTSSTRD	16 mer
D	PTPSPEPPPSVVR	13 mer
F	EGHSGPSNRARWGPRGARSH NPRNPASTAMGSSVPG	36 mer
G	FAPVLDGAVSTLLGV	15 mer
H	ESRHHPPSNPRQQPH	15 mer

Immunostaining of cultured cells

AsPC1 cells (2 × 104/well) were seeded onto a cover glass (Asahi Techno Glass, Chiba, Japan) in 24-well plates and incubated overnight. Then the old medium was changed to fresh medium containing 10 μg/mL of the indicated peptides. After incubation for 24 h, the slides were air-dried and immersed in 8% formaldehyde for 30 min. Primary antibodies were incubated overnight at 4°C. The primary antibody used was Shh (N-19; Santa Cruz Biotechnology, Santa Cruz, CA, USA) at the concentration of 1:250. Secondary antibodies (rabbit anti-goat immunoglobulin; Nichirei, Tokyo, Japan) were applied for 1 h at room temperature. After mounting in Vectorshield Mounting Medium (Vector Laboratories, Burlingame, California, USA), samples were visualized under a laser-scanning confocal fluorescence microscope (LSM-GB200 System; Olympus Optical, Tokyo, Japan).

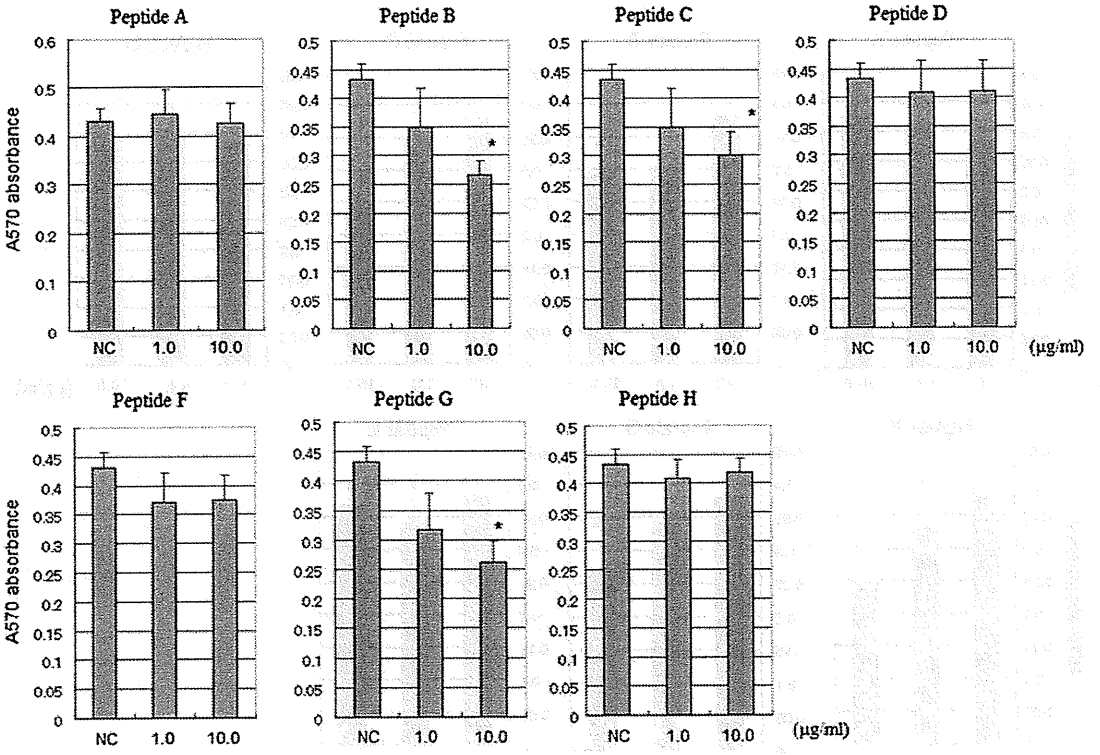

Fig. 1 Biological screening of interacting peptides using pancreatic cancer cell line AsPC1. AsPC1 cells were incubated with two concentrations of peptides, 1.0 or 10.0 μg/mL, and subjected to the 3-(4,5-dimethylthiazol-2-yl)-2,5-diphenyltetrazolium bromide (MTT) assay. Peptides B, C, and G showed a suppressive effect on cell growth in a dose-dependent manner. Results are expressed as means ± standard deviation (SD). *NC* normal control (buffer alone). $^*P < 0.05$

Animal model and peritoneal transplantation of AsPC1

The procedures followed for the animal experiments were in accordance with the guidelines for the care and use of laboratory animals of our institution or the guidelines of the National Animal Welfare Committee. Four- to six-week-old female NOD/severe combined immunodeficiency (SCID) mice were purchased from Japan SLC (Hamamatsu, Japan). The mice were housed in laminar flow cabinets under specific pathogen-free conditions in facilities approved by Kyushu University. AsPC1 or SUIT2 cells were suspended in a serum-free-RPMI/Matrigel (BD Biosciences Japan, Tokyo, Japan) mixture (1:1 volume, total 1×10^5 cells/0.4 mL) and then injected into the gluteal region of the mice with a 27-gauge needle. After tumor formation, 200 μg of peptide was injected into the tumor site with a 27-gauge needle once a day for 5 days. Tumor formation, the size of the tumors, and body weight of the mice were determined every 2 days for 46 days [22].

Statistical analysis

Student's *t*-test was used for statistical analysis. All calculations were carried out using StatView 5.0J software (Abacus Concepts, Berkeley, CA, USA). *P* values of <0.05 were considered significant [12, 23].

Results

Sequences of interacting peptides to Ptch1

Using the MIMETIC program, seven peptide sequences were designed as interacting peptides to Ptch1 (peptides A–H; Table 1).

Interacting peptides to Ptch1 suppressed pancreatic cancer cell proliferation in vitro

Peptides B, C, and G showed suppressive effects on cell growth in a dose-dependent manner (Fig. 1). We repeated the biological screening using SUIT2. Peptides B, C, F, and G suppressed SUIT2 cell growth in a dose-dependent manner (Fig. 2). This result was similar to that for AsPC1, with the exception of peptide F.

To further confirm the biological effect of the peptides as detected by the MTT assay, pancreatic cancer cells were incubated with the peptides, and subjected to Coulter counting. Consistent with the result of the MTT assay, peptides B, C, and G showed a suppressive effect on the proliferation of AsPC1 and SUIT2, and peptide F had an effect only on SUIT2 (Fig. 3a, b).

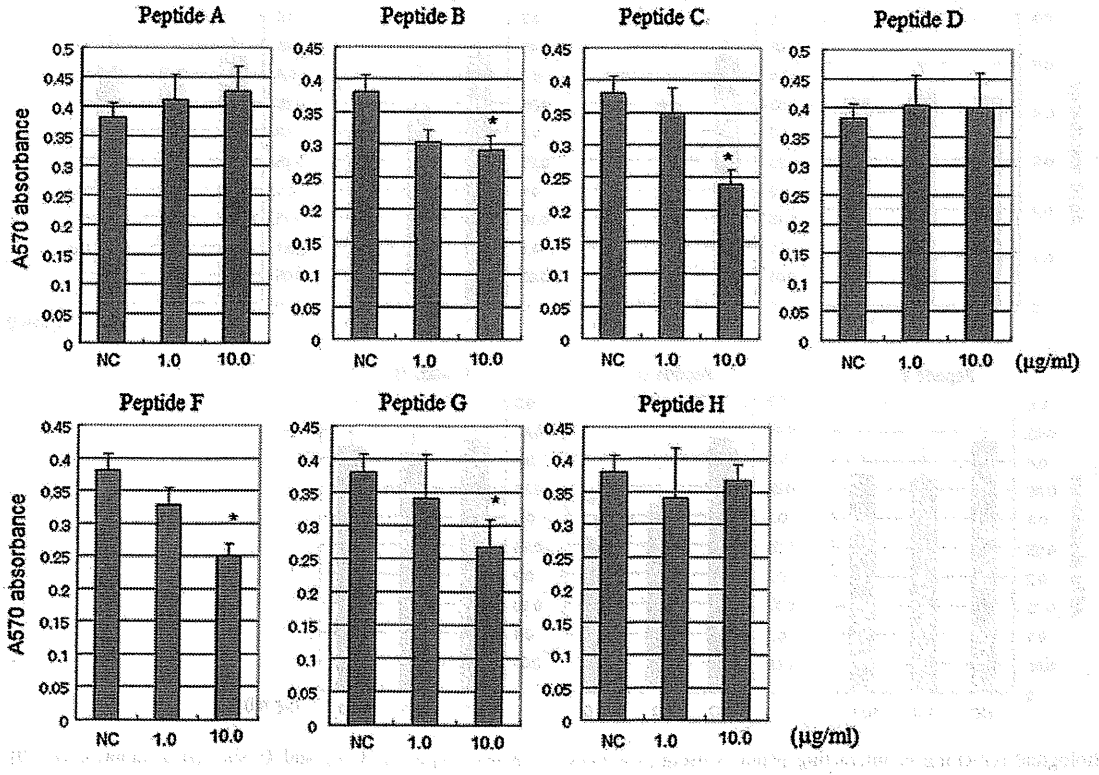

Fig. 2 Biological screening of interacting peptides using pancreatic cancer cell line SUIT2. SUIT2 cells were incubated with two concentrations of peptides, and subjected to the MTT assay. Peptides B, C, F, and G suppressed SUIT2 cell growth in a dose-dependent manner. Results are expressed as means ± SD, $^*P < 0.05$

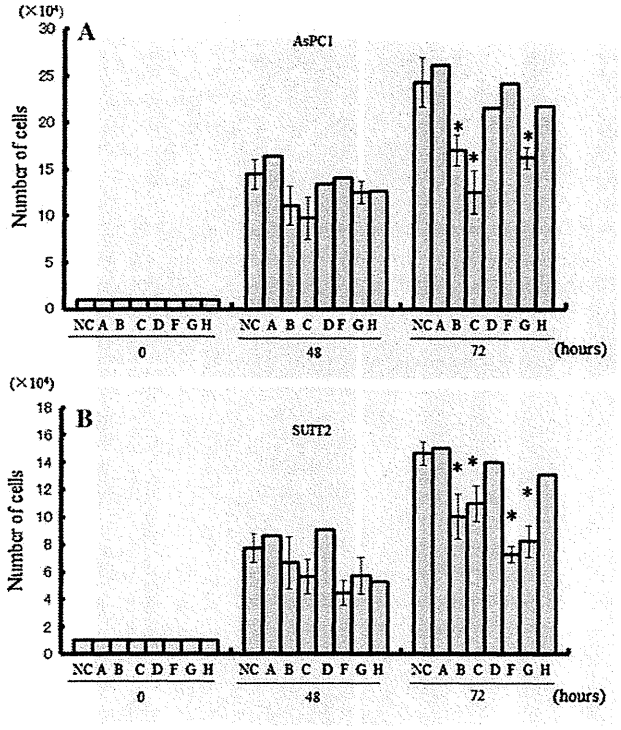

Fig. 3 Interacting peptides suppressed the proliferation of pancreatic cancer cells. Pancreatic cancer cells, AsPC1 (**a**) and SUIT2 (**b**), were incubated with the interacting peptides, and then subjected to Coulter counting. Consistent with the result of the MTT assay, peptides B, C, and G showed a suppressive effect on the proliferation of AsPC1 and SUIT2, and peptide F had an effect on SUIT2 only. Results are expressed as means ± SD. $*P < 0.05$

Interacting peptides to Ptch1 suppressed Hh signaling pathway

To confirm that the biological effect of the peptides on cancer cell growth was caused by attenuation of the activity of the Hh signaling pathway, we examined the effect of the synthesized peptides on this pathway. Because Gli1 is not only the transcription factor of the Hh signaling pathway but also a target gene of the Hh pathway, we used the Gli1 mRNA expression level as a marker of Hh pathway activity. As peptides B, C, and G had been confirmed to suppress the growth of AsPC1, we co-incubated AsPC1 with each of these peptides. Peptide A was also co-incubated with AsPC1 independently as a negative control. After a 72-h incubation,, mRNA was prepared from the cultured cells and subjected to quantitative analysis by real-time RT-PCR. As expected, the mRNA level of Gli1 was significantly suppressed by all three peptides B, C, and G, in contrast with the mRNA level of cells co-incubated with peptide A or without peptides (Fig. 4a).

As four peptides, B, C, F, and G, showed a suppressive effect on the proliferation of SUIT2, we examined the effect of these four peptides on SUIT2, and also used peptide A as a negative control. Real-time RT-PCR showed that the mRNA level of cells cultured with all four peptides, B, C, F, and G, was significantly suppressed compared with that in cells cultured with peptide A or without peptides (Fig. 4b). Our data strongly suggested that the suppressive effect of the interacting peptides to Ptch1 on tumor cell growth was induced by attenuating the activity of the Hh signaling pathway.

Interacting peptides to Ptch1 inhibited the interaction between Ptch1 and Shh

The interacting peptides to Ptch1 were too small to be stained by antibodies, so we confirmed the specificity of peptides to Ptch1 protein by the effect that peptides competitively inhibited the interaction between Ptch1 and Shh. AsPC1 cells were incubated with peptide B, C, or G. Then the staining levels of Shh around the AsPC1 cells were examined (Fig. 5). Staining levels of AsPC1 cells with peptides B, C, and G were lower than that of cells with peptide A, the control peptide. This finding supported the idea that peptides B, C, and G specifically interacted with Ptch1 at the designated docking site with Shh.

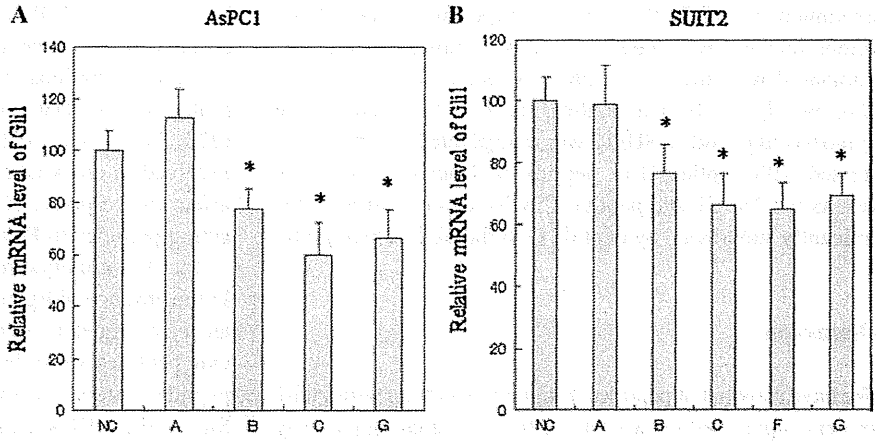

Fig. 4 Interacting peptides suppressed the activity of the hedgehog (Hh) signaling pathway. AsPC1 (**a**) and SUIT2 (**b**) cells were incubated for 72 h with the interacting peptides. The mRNA level of Gli1 was significantly suppressed by peptides B, C, and G in AsPC1 and SUIT2, and by peptide F in SUIT2. Results are expressed as means ± SD. $*P < 0.05$